


# High-Performance Thermionic Cooling Devices Based on Tilted-Barrier Semiconductor Heterostructures

Marc Bescond<sup>1,2,\*</sup> and Kazuhiko Hirakawa<sup>1,2,3</sup>

<sup>1</sup>*Institute of Industrial Science, University of Tokyo, 4-6-1 Komaba, Meguro-ku, Tokyo 153-8505, Japan*

<sup>2</sup>*LIMMS-CNRS, UMI 2820, 4-6-1 Komaba, Meguro-ku, Tokyo 153-8505, Japan*

<sup>3</sup>*Institute for Nano Quantum Information Electronics, University of Tokyo, 4-6-1 Komaba, Meguro-ku, Tokyo 153-8505, Japan*

 (Received 14 September 2020; revised 5 November 2020; accepted 10 November 2020; published 7 December 2020)

We study by means of full quantum simulations an asymmetric double-barrier semiconductor heterostructure refrigerator combining resonant tunneling filtering and thermionic emission. By varying the quantum well thickness, we first investigate the influence of the activation energy  $W$  on the coefficient of performance (COP) and cooling power. We show that the best performances are obtained when  $W$  equals the polar optical phonon energy of the material. However, we also emphasize that cooling power and the COP are severely limited by tunneling current at high bias. We then propose an original structure with a tilted potential barrier to reduce this degrading effect. Quantum simulations demonstrate that cooling properties of such tilted barrier devices are significantly improved in the out-of-equilibrium regime, where the thermionic cooling concept offers its best efficiency.

DOI: [10.1103/PhysRevApplied.14.064022](https://doi.org/10.1103/PhysRevApplied.14.064022)

## I. INTRODUCTION

The self-heating effect represents one of the most important technological issues in opto- and nanoelectronics. It results from the thermalization of hot carriers generated by high electric fields, leading to an on-chip power density largely above  $100 \text{ W/cm}^2$  and to lattice temperatures higher than four hundred kelvins [1,2]. Such high temperatures induce significant reduction in efficiency [3] and reliability [4] of the devices. Unfortunately, thermal management is becoming even more challenging in recent three-dimensional (3D) integrated circuit architectures due to complex electrical interconnects among different device layers.

The refrigeration of electronic systems is most often based on liquid or air (fans) active cooling techniques [5]. Such approaches, which cool the entire system, do not face the problems of temperature nonuniformity and localized hot spots created by the nanoscaling of electronic devices. Moreover, these techniques are also extremely power consuming. For example, 40% of the energy consumed by data centers is devoted to cooling [6]. All these features make solving integrated circuit cooling one of the major scientific, technological, and environmental tasks in a context of energy resource shortage [7,8].

Innovative cooling technologies, emerging from solid-state physics, are therefore urgently needed. So far, most

of the studies are based on the thermoelectric Peltier effect. Thermoelectricity is a relevant solution since it is a “green” and robust method working at small scales. However, thermoelectric cooling operates in the near-equilibrium regime. Electrons propagate diffusively through the materials, returning part of their energy to the lattice and reducing the cooling efficiency. We therefore investigate nanoscaled cooling devices in which the transport of electrons and phonons become strongly ballistic and whose working principle applies far from equilibrium. This is the field of thermionic cooling that leads to higher cooling efficiency than in conventional thermoelectric devices [9].

Thermionic cooling devices were first proposed in the 1950s [10] and were characterized by two metals separated by a vacuum region. The working principle was based on the fact that electrons with high thermal energy (greater than the work function of the metal) can escape from the metal. Electrons thermionically emitted from the cathode then transfer their kinetic energies to the anode to give rise to refrigeration in the cathode [11]. However, metal-vacuum-metal-based thermionic refrigerators were shown to mainly operate at high temperatures (greater than 700 K). Room-temperature refrigerators using this concept were really investigated in the 1990s with the emergence of semiconductor heterostructures in which the quasiballistic transport of electrons could occur [12–14]. The central vacuum region was replaced by a semiconductor heterostructure including one or several potential barriers. Lattice cooling of approximately 1 to 5 K was observed

\*bescond@iis.u-tokyo.ac.jp

at 300 K [15–17]. However, due to the strong exploratory character of the topic, the reported performances suffered from a lack of theoretical insights. The investigation of thermionic cooling devices indeed requires extensive theoretical and computational quantum modeling capable of describing electron and phonon transport at the nanometer scale. In order to capture the key aspects of the physics, we use the quantum nonequilibrium Green’s function (NEGF) method. Our full numerical quantum simulations are able to take into account the thermal effects by self-consistently coupling the electron transport equations expressed within the NEGF formalism with the heat equation [18].

We focus on double-barrier asymmetric heterostructures since we recently demonstrated that such devices can efficiently act on electronic and phononic bath refrigeration [18,19]. We consider the device shown in Fig. 1. It illustrates the band diagram of the asymmetric double-barrier heterostructure that couples “tunnel injection” and “thermionic extraction.” In this structure, “cold” electrons are injected from the emitter into the GaAs quantum well (QW) via a resonant tunneling effect through a thin potential barrier (referred to as the “emitter barrier”). The role of the emitter barrier is to filter injected electrons and to concentrate the cooling in the QW. “Hot” electrons are removed from the QW through a thermionic process above the thick (Al, Ga)As alloy (referred to as the “collector barrier”), extracting the activation energy  $W$  from the lattice via phonon absorption. Electrons are then relaxed in the collector by emitting phonons. As a result, the QW cools and the collector heats.

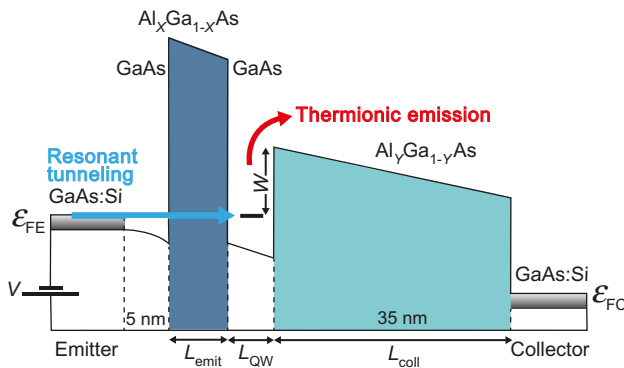


FIG. 1. Sketch of the considered asymmetric double-barrier heterostructure. For all the considered devices, doping in the emitter and the collector is  $10^{18} \text{ cm}^{-3}$ . Here  $L_{\text{QW}}$  denotes the quantum well thickness and  $W$  denotes the activation energy, defining the gap between the QW state and the top of the collector barrier. The thicknesses of the emitter and collector barriers are  $L_{\text{emit}} = 2 \text{ nm}$  and  $L_{\text{coll}} = 35 \text{ nm}$ , with  $X = 0.4$  and  $Y = 0.15$  their respective aluminum concentrations, corresponding to barrier heights of 0.32 and 0.12 eV.  $\epsilon_{\text{FE}}$  and  $\epsilon_{\text{FC}}$  are the Fermi levels of the emitter and collector respectively.

In this work, we first report an extensive study of the impact of  $W$  by varying the QW thickness ( $L_{\text{QW}}$ ) on the electrical and cooling properties. We demonstrate that the best cooling characteristics are obtained for  $W$  close to the polar optical phonon energy of the material,  $\hbar\omega_{\text{LO}}$ . Although promising, the performances are found to degrade at high bias due to the tunneling of electrons across the collector barrier. We therefore propose an original structure with a tilted potential in the collector barrier that is able to reduce this parasitic tunnel escape of electrons in the QW.

The paper is organized as follows. In Sec. II we describe the electronic quantum transport and heat transport models. In Sec. III we discuss the influence of the activation energy  $W$  by varying  $L_{\text{QW}}$  in terms of the current characteristics, local density of states (LDOS), current spectra, and coefficient of performance (COP). From these numerical investigations, we propose an original structure with a tilted potential profile in the collector barrier and demonstrate its superiority over the cooling properties of the initial device. We present our concluding remarks in Sec. IV.

## II. THEORETICAL APPROACH

In order to theoretically study such a quantum device, we couple both electron and phonon transport.

### A. Quantum transport for electrons

Electron transport is described via the NEGF quantum formalism [20,21]. Transport equations are expressed within the effective mass approximation to implement a 1D quantum simulator along the heterostructure growth direction ( $x$ ). The single-band effective mass Hamiltonian describes the  $\Gamma$  valley of the conduction band of the III-V semiconductors. As the considered structure is translationally invariant in the in-plane  $y$  and  $z$  directions, Born–von Karman periodic boundary conditions are applied on the transverse wave vector component  $k_t$  such that  $k_t = n_{k_t} 2\pi/L_t$ , with  $L_t = 50 \text{ nm}$  and  $n_{k_t}$  an integer indexing the transverse modes whose degeneracies are equal to  $\pi(2 \times n_{k_t} + 1)$  [22]. In the following, we summarize the main features of the NEGF approach in matrix notation. We first define the retarded Green’s function at energy  $E$  for each transverse mode  $k_t$ ,

$$G_{k_t}^r = [(E - V)I - H_{k_t} - \Sigma_{L,k_t}^r - \Sigma_{R,k_t}^r - \Sigma_{S,k_t}^r]^{-1}, \quad (1)$$

where  $I$  is the identity matrix,  $H_{k_t}$  denotes the effective mass Hamiltonian for the transverse mode  $k_t$ ,  $V$  is the electrostatic potential energy, and  $\Sigma_{L/R}^r$  and  $\Sigma_S^r$  are the retarded self-energies for the left and right semi-infinite device contacts [23] and scattering mechanisms, respectively.

From the retarded Green's function, the lesser and greater Green's functions are then obtained as

$$G_{k_t}^{\lessgtr} = G_{k_t}^r (\Sigma_{L,k_t}^{\lessgtr} + \Sigma_{R,k_t}^{\lessgtr} + \Sigma_{S,k_t}^{\lessgtr}) G_{k_t}^{r\dagger}, \quad (2)$$

where the  $\Sigma^{\lessgtr}$  are the lesser and greater self-energies, related to their retarded counterpart by

$$\Sigma^r = \frac{1}{2}[\Sigma^> - \Sigma^<]. \quad (3)$$

Only acoustic and polar optical phonon interactions are considered, since nonpolar-optical phonons turn out to be negligible in the semiconductors considered in this work [24]. Interface roughness scattering is also assumed to be negligible with respect to polar optical phonon scattering. We mention in particular the work of Lake *et al.* [25], who clearly showed that polar optical phonon scattering is significantly larger than the interface roughness contribution in GaAs/AlAs RTDs. Interaction self-energies are calculated within the self-consistent Born approximation (SCBA) [26–28]. In our approach, the acoustic phonon (AC) and polar optical phonon (POP) baths locally follow a Bose-Einstein distribution, and are therefore assumed at equilibrium. On the other hand, acoustic and optical phonons cannot be assumed at equilibrium with respect to each other, as the net anharmonic decay of optical phonons into acoustic phonons plays a fundamental role in the thermal transport [29]. This is taken into account in our model by defining, at each position of the domain, two different temperatures,  $T_{AC}$  and  $T_{POP}$  in the acoustic  $\Sigma_{AC,k_t}^{\lessgtr}$  and polar optical  $\Sigma_{POP,k_t}^{\lessgtr}$  phonon self-energies, respectively. As detailed in the next subsection, these temperatures are self-consistently computed by coupling the electron transport equations with the heat equation.

Interactions with both acoustic and polar optical phonons are here assumed to be local and we then consider only the diagonal part of the matrix self-energies. Such an approximation has been demonstrated to be valid for acoustic phonons down to very low temperatures [30]. To describe the POP, we adopt the diagonal expression of the scattering self-energy recently proposed as an effective description of their long-range interactions [31]. For a given wave vector  $k_t$ , it can be shown that

$$\begin{aligned} \Sigma_{POP,k_t}^{\lessgtr}(j,j,E) &= \frac{\lambda M^2}{2\pi S} \sum_{k'_t} \{ [n_L(j) + 1] G_{k'_t}^{\lessgtr}(j,j,E \pm \hbar\omega_{LO}) \\ &+ [n_L(j)] G_{k'_t}^{\lessgtr}(j,j,E \mp \hbar\omega_{LO}) \} \\ &\times \int_{\pi/L_t}^{\pi} \frac{\pi(2n_{k'_t} + 1)}{\sqrt{(k_t - k'_t \cos \theta)^2 + (k'_t \sin \theta)^2}} d\theta, \end{aligned} \quad (4)$$

where  $n_L(j) = (e^{\hbar\omega_{LO}/[k_B T_{POP}(j)]} - 1)^{-1}$ ,  $M^2 = 2\pi \hbar\omega_{LO} e^2 (1/\epsilon_\infty - 1/\epsilon_0)$ ,  $\theta$  is the angle between  $k_t$  and  $k'_t$ ,  $S = \pi L_t^2$ ,

and  $\hbar\omega_{LO} = 35$  meV. The index  $j$  indicates the  $x$  position along the discretized domain, while  $M$  is the Fröhlich factor in which  $\epsilon_0$  and  $\epsilon_\infty$  represent the static and high-frequency dielectric permittivities, respectively. Finally,  $\lambda$  is a scaling factor that takes into account the diagonal approximation. The value  $\lambda = 8$  used in this paper has been obtained within the comprehensive and physically based analytical model proposed in Ref. [31].

The total phonon scattering SCBA self-energy  $\Sigma_{S,k_t}^{\lessgtr}$  for a given mode  $k_t$  can then be decomposed as

$$\Sigma_{S,k_t}^{\lessgtr} = \Sigma_{AC,k_t}^{\lessgtr} + \Sigma_{POP,k_t}^{\lessgtr}. \quad (5)$$

Once the lesser and greater Green's function  $G_{k_t}^{\lessgtr}$  of each mode  $k_t$  is determined, the electron density can be calculated [26]:

$$n_j = -2 \frac{i}{2\pi} \sum_{k_t} \pi(2n_{k_t} + 1) \int_{-\infty}^{+\infty} G_{k_t}^<(j,j;E) dE, \quad (6)$$

$$= -i \int_{-\infty}^{+\infty} G^<(j,j;E) dE \quad (7)$$

with  $G^<(j,j;E) = \sum_{k_t} (2n_{k_t} + 1) G_{k_t}^<(j,j;E)$ . The carrier current density flowing from position  $j$  to  $j + 1$  is calculated from the off-diagonal elements  $(j, j + 1)$  of  $G_{k_t}^<(i,j;E)$  as

$$\begin{aligned} J_{j \rightarrow j+1} &= \int_{-\infty}^{+\infty} dE \frac{e}{\hbar} \sum_{k_t} \frac{2n_{k_t} + 1}{S} [H_{j,j+1} G_{k_t}^<(j+1,j;E) \\ &- G_{k_t}^<(j,j+1;E) H_{j+1,j}] \\ &= \int_{-\infty}^{+\infty} \mathcal{J}_{j \rightarrow j+1}(E) dE, \end{aligned} \quad (8)$$

where  $H_{j,j+1}$  denotes to the nearest-neighbor hopping term in the discretized tight-binding-like Hamiltonian and  $\mathcal{J}_{j \rightarrow j+1}(E)$  is the current density spectrum [in A/(m<sup>2</sup> eV)]. From Eq. (8) we can deduce the corresponding electronic energy current [34]

$$J_{j \rightarrow j+1}^E = \int_{-\infty}^{+\infty} E \mathcal{J}_{j \rightarrow j+1}(E) dE. \quad (9)$$

In practice, the set of Eqs. (1)–(5) is solved self-consistently using a recursive algorithm [23,35] until the criteria of convergence for both the electron density and carrier current density are reached. The potential energy  $V$  is self-consistently determined by nonlinearly coupling the transport Eqs. (1)–(5) with the Poisson equation through the electron density. In this study, band offsets are calculated based on the values reported in Ref. [32]. The other parameters used in the NEGF code are reported in Table I.

TABLE I. Principal NEGF parameters used in this work.

	$m_{\Gamma}^*(\text{GaAs})$	$m_{\Gamma}^*(\text{AlAs})$	$m_{\Gamma}^*(\text{Al}_x\text{Ga}_{1-x}\text{As})$	$\hbar\omega_{\text{LO}}$ (meV)	$\epsilon_0$	$\epsilon_{\infty}$
	0.067	0.15	$xm_{\Gamma}^*(\text{AlAs})+(1-x)m_{\Gamma}^*(\text{GaAs})$	35	12.9	10.89
Ref.	[32]	[32]	[32]	[33]	[33]	[33]

### B. Heat transport model

Heat transport is described by solving the 1D heat equation along the  $x$  direction. The discretized heat equation at site  $j$  reads

$$\left\{ -\frac{\partial}{\partial x} \left[ \kappa_{\text{th}}(x) \frac{\partial}{\partial x} T_{\text{AC}}(x) \right] \right\}_j = Q_j, \quad (10)$$

where  $\kappa_{\text{th}}$  is the thermal conductivity. It is taken equal to the GaAs bulk value [46 W/(m K)] in the device, except in the QW region, where it is set to 4 W/(m K) in order to take into account the thermal resistance associated with the interface between different layers [36,37]. The heat equation considers the temperature of acoustic phonons, since they have a larger velocity than their polar optical counterparts and are mainly responsible for heat transport [38]. Left and right reservoirs are assumed to be at the thermodynamic equilibrium at  $T_{\text{AC}} = 300$  K. This assumption corresponds to considering massive contacts with a sufficiently high thermal capacitance. We denote by  $Q_j$  the volumetric source term that corresponds to the cooling power density (in W/m<sup>3</sup>) generated by electron-phonon interactions. In the framework of the previously described electron transport formalism, it can be computed as [34,39]

$$Q_j = -\nabla_j \cdot J^E. \quad (11)$$

A negative value of  $Q_j$  corresponds to an energy transfer from the lattice to electrons, while a positive value describes the reverse phenomenon. From a physical point of view, electrons lose or increase their energy by scattering with polar optical phonons. In turn, optical phonons decay into acoustic phonon modes, which sustains the thermal energy propagation along the device. In stationary conditions, the power transfer from optical to acoustic phonons must be equal to the cooling power density (CPD)  $Q_j$  defined above. Within a relaxation time approximation [29], we can thus write

$$\frac{[T_{\text{POP}}(j) - T_{\text{AC}}(j)]C_{\text{POP}}}{\tau_{\text{POP} \rightarrow \text{AC}}} = Q_j, \quad (12)$$

where  $\tau_{\text{POP} \rightarrow \text{AC}}$  is the relaxation time of polar optical phonons decaying into acoustic phonons ( $\tau_{\text{POP} \rightarrow \text{AC}} = 4.16 \times 10^{-12}$  s) [40] and  $C_{\text{POP}}$  is the thermal capacitance of the polar optical-phonons per unit volume [ $C_{\text{POP}} = 1.72 \times 10^6$  J/(m<sup>3</sup> K)] [40]. The numerator of the left-hand side expresses the average energy per unit volume exchanged

between the polar optical and acoustic phonon baths in an interval  $\tau_{\text{POP} \rightarrow \text{AC}}$ . Equation (12) allows us to compute  $T_{\text{POP}}(j)$  from knowledge of  $Q_j$  and  $T_{\text{AC}}(j)$ .

The computed values of  $T_{\text{AC}}$  and  $T_{\text{POP}}$  are substituted into Eq. (5). This establishes the coupling between the heat equation and the electron transport equations. The heat equation is iteratively solved together with the transport equations and the Poisson equation, until a global self-consistency is achieved.

### III. RESULTS AND DISCUSSION

In this section we first analyze the influence of  $W$ , by varying the QW thickness, on the cooling properties. We report a comprehensive study on the involved physical effects and show that the double-barrier structure provides its best features when  $W$  is close to the polar optical phonon frequency of the material,  $\hbar\omega_{\text{LO}}$ . However, even in this configuration, the device undergoes performance degradations at high bias due to tunneling current across the collector barrier. Based on this observation, we then propose a structure with a tilted collector barrier, leading to a significant improvement in the cooling characteristics.

Cooling properties clearly depend on the activation energy  $W$ . In the following, we focus on the influence of  $W$  by varying the QW thickness,  $L_{\text{QW}}$ . For instance, increasing  $L_{\text{QW}}$  reduces the position of the quasilocalized state in the QW and leads to an increase in  $W$ .

In Fig. 2 we show the current characteristics obtained for four  $L_{\text{QW}}$  varying from 4 to 12 nm. We can see that the current decreases when increasing the QW thickness. More precisely, the device with  $L_{\text{QW}} = 4$  nm provides the highest current density for the entire bias range. Increasing the QW thickness to 5, 6, and 12 nm induces a current decrease up to 40%, 55%, and 70%, respectively.

To understand this dependance, in Fig. 3 we show the LDOS (top row) and the current spectra (bottom row) for  $L_{\text{QW}} = 4, 6, 12$  nm at  $V = 0.1$  V.

For  $L_{\text{QW}} = 4$  nm, the quasilocalized state is quite high in the QW, leading to an activation energy  $W$  of 40 meV [Fig. 3(a)]. Electrons can then easily escape from the QW via phonon absorption ( $\hbar\omega_{\text{LO}} = 35$  meV in GaAs) and hence generate a high current density [Fig. 3(d)]. When increasing  $L_{\text{QW}}$  to 6 nm,  $W$  attains 66 meV [Fig. 3(b)], which significantly reduces the thermionic current. In particular, we clearly see in Fig. 3(e) two components of the current spectrum: one resulting from the resonant tunneling across the emitter barrier towards the QW state, and a



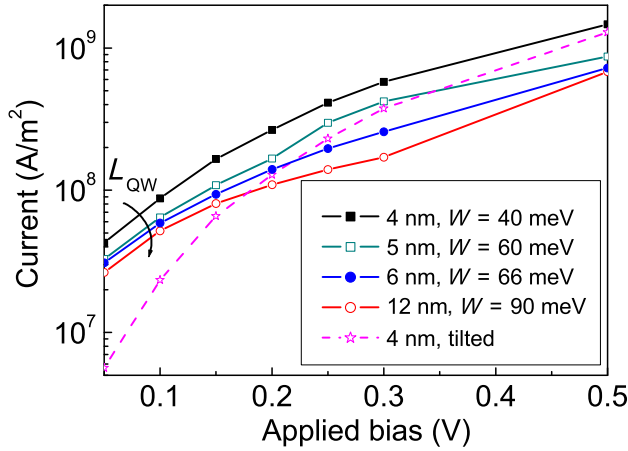


FIG. 2. Influence of  $W$  on the current density by varying the quantum well thickness,  $L_{\text{QW}}$ , as a function of the applied bias. Four  $L_{\text{QW}}$  are considered: 4 nm (filled squares), 5 nm (open squares), 6 nm (filled circles), and 12 nm (open circles). The current density obtained with a tilted collector barrier is also represented for  $L_{\text{QW}} = 4$  nm (stars). In this latter structure, the aluminum concentration  $Y$  varies uniformly from 0.15 at the QW edge to 0.3 at the collector edge in constant steps of 5 nm.

second resulting from the QW above the collector barrier. Because of the thick collector barrier, the resonant tunneling component indeed ends in the QW. For  $L_{\text{QW}} = 12$  nm, the first bound state continues to decrease in the well, leading to  $W = 90$  meV. Moreover, the second quasi-localized state now enters the QW [Fig. 3(c)], inducing a second thermionic component around 0.12 eV in the current spectrum [Fig. 3(f)]. This second conducting channel is however not enough to compensate for the rise of  $W$  and the total current keeps decreasing.

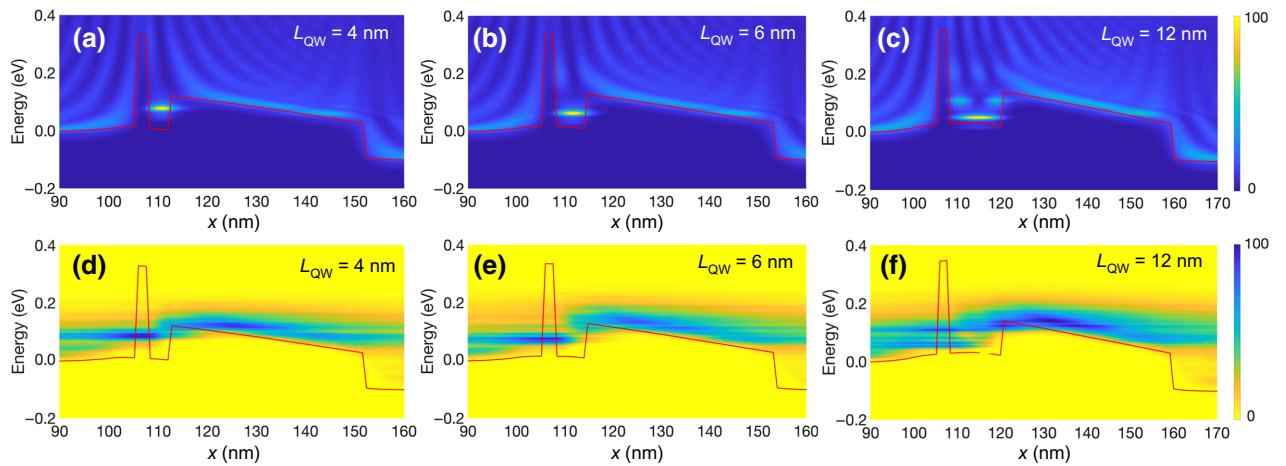


FIG. 3. Top row: LDOS for (a)  $L_{\text{QW}} = 4$  nm; (b)  $L_{\text{QW}} = 6$  nm; (c)  $L_{\text{QW}} = 12$  nm, calculated for  $V = 0.1$  V. Bottom row: (d), (e), and (f) are current spectra corresponding to (a), (b), and (c). Solid red lines indicate the potential profile along the devices. The origin of the energy scale is the Fermi level of the emitter,  $\varepsilon_{\text{FE}}$ .

In Fig. 4(a) we show the cooling power  $J_Q$  for the three previously considered  $L_{\text{QW}}$ . We obtain  $J_Q$  by integrating over  $x$  the negative part of the cooling power density  $Q_j$  [Eq. (11)]. According to the definition of  $Q_j$ , a negative (positive) value of  $Q_j$  indicates a cooling (heating) of the lattice. We then only integrate the negative component of  $Q_j$  in order to obtain the cooling power of the entire device. Also integrating the positive component of  $Q_j$  would systematically give a final positive value equal to the applied electrical power ( $P_{\text{elec}} = JV$ ), due to energy conservation. We remark that the entire device (central region plus contacts) always heats more than it cools, but the aim is to locally efficiently cool the QW and to extract the heat as far as possible from it, in the collector region. This is unfortunately inherent to all thermionic cooling and thermoelectric devices. The cooling power presents the same general feature for the three structures. Starting from small values at low bias, it reaches a maximum at  $V = 0.3$  V.

Figure 5(a) sheds light on this trend. It shows the cooling power density for  $L_{\text{QW}} = 4$  nm at  $V = 0.1$  and 0.3 V. We see that the negative component (corresponding to the cooling power) is higher at  $V = 0.3$  V. In particular, the two dips located just before the emitter barrier and in the QW are enhanced. These two dips correspond to phonon absorption before the emitter barrier and in the QW, respectively. Indeed, as shown in the LDOS of Fig. 5(b), the energy interval between the bottom of the conduction band in the emitter and the QW state is equal to  $W$  (approximately 40 meV). This value is also very close to the polar optical phonon energy in GaAs ( $\hbar\omega_{\text{LO}} = 35$  meV). Electrons in the emitter region can then be transmitted across the device by absorbing sequentially two polar optical phonons. This is also why a device with  $L_{\text{QW}} = 4$  nm gives the highest cooling power. For higher  $W$ , several phonons are required to extract the electrons from the QW, reducing

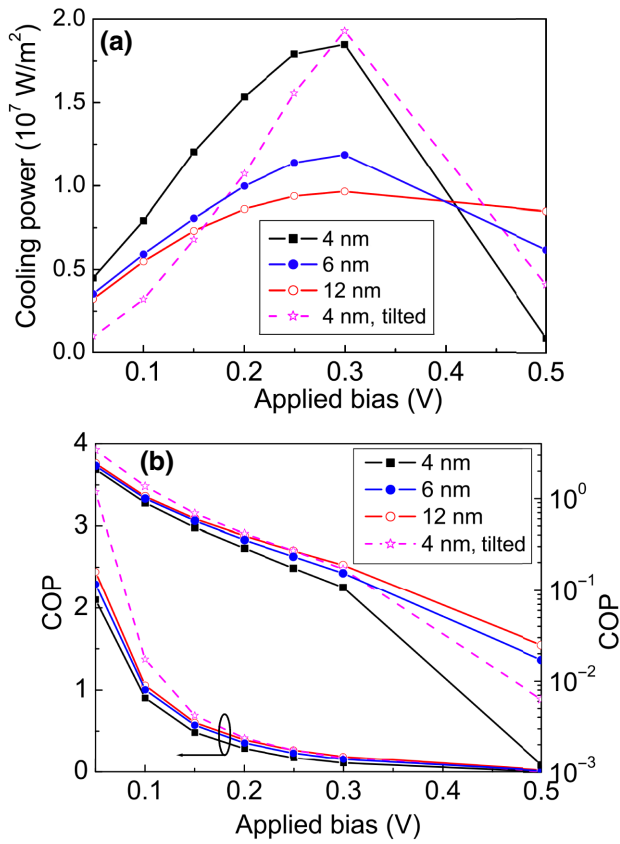


FIG. 4. (a) Cooling power ( $J_Q$ ) and (b) COP for three  $L_{\text{QW}}$ : 4 nm (filled squares), 6 nm (filled circles), and 12 nm (open circles). Parameters of the tilted structure with  $L_{\text{QW}} = 4$  nm are also shown. In the tilted device, the collector barrier has an aluminum concentration varying from 0.15 at the QW edge to 0.3 at the collector edge in constant steps of 5 nm.

the current and therefore the power. At larger bias, the QW state first aligns and then goes below the bottom of the conduction band in the emitter. In that regime, electrons need to emit phonons before reaching the QW states. The current keeps increasing, but phonon absorption and  $J_Q$  are drastically reduced. The case of  $L_{\text{QW}} = 12$  nm is slightly different since the cooling power is not reduced at  $V = 0.5$  V. This is due to the presence of the second bound state through which transport can occur and which goes below the bottom of the conduction band at higher bias. We do not discuss this phenomenon in more detail since it does not significantly influence the refrigeration properties.

In Fig. 4(b) we show the related COP, defined as the ratio of  $J_Q$  by the applied power ( $P_{\text{elec}} = JV$ ). For all the structures, the COP decreases with the bias. This feature can be simply explained by assuming that cooling power is proportional to  $WJ$ . This rough approximation is valid in the case where most of the electrons are extracted at the top of the collector barrier. With the distribution of electrons in the QW following the Maxwell-Boltzmann statistics, the contribution of states above  $W$  decreases exponentially,

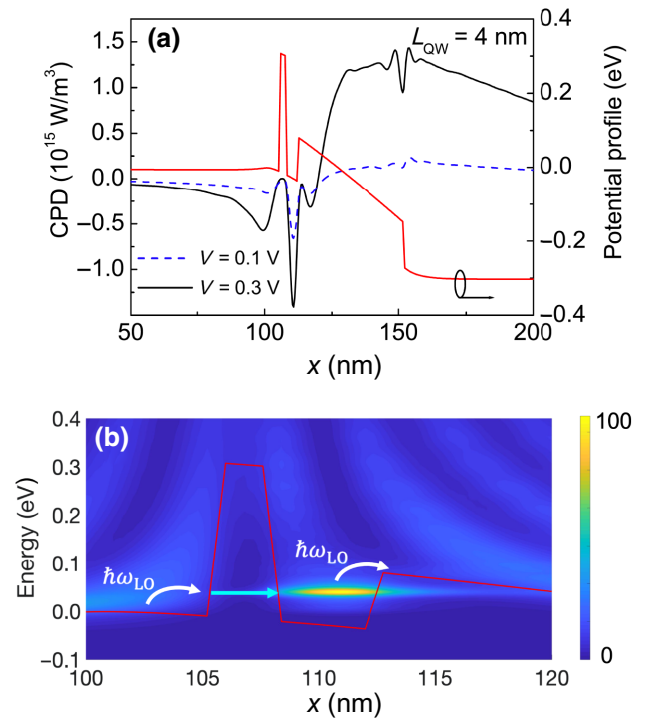


FIG. 5. (a) CPD for  $V = 0.1$  V (dashed line) and  $V = 0.3$  V (solid line); (b) LDOS in the QW region at  $V = 0.3$  V. In both panels, the solid red line represents the energy potential profile. Here  $L_{\text{QW}} = 4$  nm.

and should be rather small. We indeed demonstrated both experimentally and theoretically in Ref. [19] that electron extraction from the QW mainly occurs at the top of the collector barrier, leading to an evaporative cooling effect. When applying a bias, hot electrons are extracted from the QW and the remaining electrons rethermalize at a lower temperature. Such an effect results from the modification of the electron momentum in the QW due to elastic interactions with acoustic phonons. All these lead us to think that an electron in the QW absorbs, on average, an energy equal to  $W$ . The COP can then be written as  $J_Q/P_{\text{elec}} = (WJ)/(JV) = W/V$ , which appears to be inversely proportional to  $V$ . At a given bias, the COP should also be the weakest for devices with the smallest  $W$ . This is indeed the case since devices with  $L_{\text{QW}} = 4$  nm and  $L_{\text{QW}} = 12$  nm report the worst and best COPs, respectively.

In terms of performances, the COP goes from less than 1% at  $V = 0.5$  V up to 250% at  $V_{\text{RL}} = 0.05$  V. Such high COP values for low bias is physically sound as long as the integration of the cooling power density over the whole device remains equal to  $P_{\text{elec}}$ . It also emphasizes the general dilemma of the cooling devices: having a high COP but almost no power at low bias or having high power but a low COP at high bias. This tendency is still valid for the different  $L_{\text{QW}}$ . We can see that the thickness providing the highest cooling power (i.e.,  $L_{\text{QW}} = 4$  nm) presents the lowest COP. The opposite is also true.

We can finally note that the COP does not decrease linearly with the applied voltage, as predicted by the simple model. Indeed, the triangular shape of the collector barrier in the high voltage regime induces a tunneling effect that causes the actual COP to deviate from this simple model. As shown in Fig. 6(a), the tunneling component, indicated by the red arrow, reduces the effective  $W$  and accelerates the degradation of the COP. In order to attenuate this degrading effect, we propose an original structure with a tilted collector barrier.

To weaken this effect, we progressively increase the aluminum concentration in the collector barrier such that the potential in this region becomes positively tilted at equilibrium, generating an additional barrier. We then take a device with  $L_{\text{QW}} = 4$  nm in which the collector barrier has an aluminum concentration varying from 0.15 at the QW edge to 0.3 at the collector edge in constant steps of 5 nm. The obtained cooling power and COP are also shown in Figs. 4(a) and 4(b), respectively. We can see that the tilted device provides a better COP over the entire bias range (by at least 60%) with respect to the conventional structure with the same  $L_{\text{QW}}$ . Indeed, the tilted collector barrier reduces the tunneling effect and increases the quantity of energy extracted by each electron, leading to better efficiency. On the other hand, the comparison of the cooling power has two regimes. At low bias (i.e.,  $V < 0.3$  V) the conventional device performs better while the

tilted structure is superior at higher voltage. This behavior is explained by the current characteristics of the tilted structure, which is also shown in Fig. 2. Because of the additional potential height in the collector barrier, the tilted device presents a much weaker current. This reduction is more important at low bias when the additional barrier is larger. When increasing the bias, the tilted collector barrier is progressively removed and the current densities of the two structures approach one another. The applied bias  $V = 0.3$  V corresponds to the tipping point where the cooling power equals that of the conventional structure. By comparing Figs. 6(a) and 6(b) we can also see that the tunneling component of the current spectrum is less dominant in the tilted structure. The red arrows in Fig. 6(b) show that the tilted potential allows the shifting up of the current spectrum above the collector barrier. We finally note that the weak current density provided by the tilted device is another great advantage since it allows us to reach the highest cooling power and COP with a much lower power consumption ( $P_{\text{elec}} = JV$ ).

To summarize, at high bias, i.e., when the thermionic cooling structures are the most relevant, the tilted device provides similar cooling power (even a bit higher) while improving the COP by at least 60% with respect to that of the conventional structure. Moreover, the smaller current density of the tilted device is another advantage in terms of power consumption. We should mention that properties of the tilted device strongly depend on the profile of the collector barrier. As such, the choice of the III-V compound is crucial to determine the operational efficiency. In the present work, (Al, Ga)As is considered as a proof of concept, since the growth of this material is technologically very well established. However, the aluminum content should be less than 0.35 in order to avoid electron scattering between the  $\Gamma$  and  $X$  valleys, and to maintain good electronic transport. This hinders a comprehensive assessment of the performances of a fully optimized structure. One could have a better clue of the expected final specifications by considering other III-V compounds, such as InAs and AlSb, whose conduction band offsets can be much larger than those of (Al, Ga)As, while keeping excellent transport properties. This is however outside the scope of the present work.

Finally, we give more general indications to improve the refrigeration properties of the device for future developments. As discussed previously, the QW is cooled, but the collector region heats. There is therefore a risk of heat backflow towards the QW. One solution to handle this detrimental effect is to consider a material in the collector barrier with a very weak electron-phonon coupling and a low thermal conductivity. We could also consider in this region a superlattice structure since it is known that thermal conductivity of semiconductor superlattices is strongly reduced (due to interface scattering) with respect to the bulk values of their constituents [41]. On the contrary,

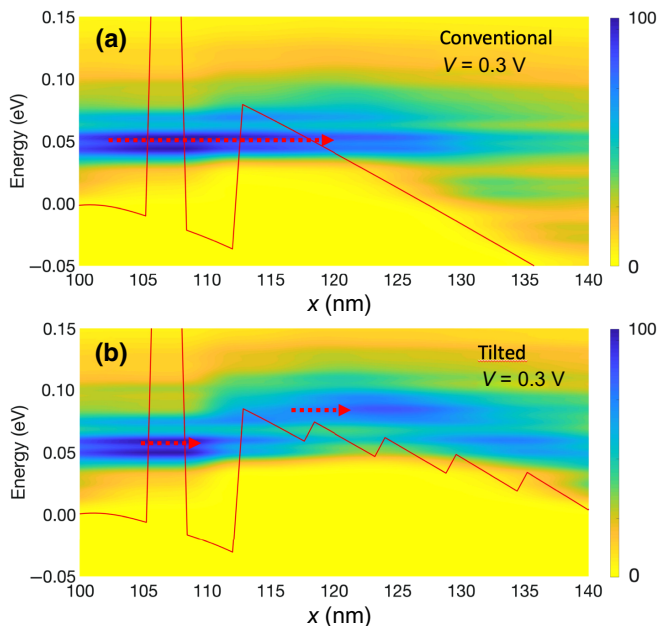


FIG. 6. Current spectra for (a) the conventional structure with  $Y = 0.15$  and (b) the tilted structure with  $Y$  varying from 0.15 to 0.3 in steps of 5 nm. The solid red lines represent the energy potential profile while red arrows indicate the electron flux through and above the collector barrier. Here  $L_{\text{QW}} = 4$  nm and the applied bias is  $V = 0.3$  V.

reservoirs should have a high thermal conductivity in order to efficiently remove heat outside the device. In the QW, cooling performances could also be improved by choosing a material with a strong electron-phonon coupling to absorb the highest power from the lattice. Lastly, we mention that the thickness of the emitter barrier,  $L_{\text{emit}}$ , essentially controls the density of injected electrons in the QW. Therefore, the physical mechanisms and the general conclusions presented in this work would not be affected by considering different thicknesses.

#### IV. CONCLUSIONS

In this work, we theoretically investigate the performances of an asymmetric double-barrier thermionic cooling device. By varying  $L_{\text{QW}}$ , we first demonstrate that both the COP and cooling power are highly dependent on the activation energy  $W$ . We show that the highest cooling power is obtained with an activation energy  $W$  close to the polar optical phonons frequency (i.e., approximately 35 meV in GaAs). When  $W$  is above this value, the COP is slightly higher but the cooling power is substantially degraded. Moreover, it turns out that tunneling current across the collector barrier is very detrimental. In order to reduce this degrading effect, we propose a structure with a tilted collector barrier by progressively increasing the aluminum concentration in this region. We show that such a device improves the COP over the entire bias range while providing the same cooler power and requiring a much lower power consumption. Therefore, the present low-energy-injection/high-energy-extraction structure coupled with a tilted potential barrier may lead to the conception of thermionic nanodevices of crucial technological interest, providing unprecedented refrigeration properties.

#### ACKNOWLEDGMENT

We are very grateful to Gerald Bastard for fruitful discussions about the influence of the activation energy. We also thank the Kakenhi C2C of the JSPS for supporting this work.

- 
- [1] R. Gaska, A. Osinsky, J. W. Yang, and M. S. Shur, Self-heating in high-power AlGaIn-GaN HFETs, *IEEE Electron. Dev. Lett.* **19**, 89 (1998).
  - [2] E. Pop and K. E. Goodson, Thermal phenomena in nanoscale transistors, *J. Electron. Packag.* **128**, 102 (2006).
  - [3] Reto Rhyner and Mathieu Luisier, Minimizing self-heating and heat dissipation in ultrascaled nanowire transistors, *Nano Lett.* **16**, 1022 (2016).
  - [4] Jayanth Srinivasan, Sarita V. Adve, Pradip Bose, and Jude A. Rivers, in *Dependable Systems and Networks, 2004 International Conference on* (IEEE, Florence, Italy, 2004) p. 177.

- [5] S. G. Kandlikar, Review and projections of integrated cooling systems for three-dimensional integrated circuits, *J. Electron. Packag.* **136**, 024001 (2014).
- [6] M. Avgerinou, P. Bertoldi, and L. Castellazzi, Trends in data centre energy consumption under the european code of conduct for data centre energy efficiency, *Energies* **10**, 1470 (2017).
- [7] G. I. Meijer, Cooling energy-hungry data centers, *Science* **328**, 318 (2010).
- [8] C. Wang, C.-Y. Li, M. P. Hasselbeck, B. Imangholi, and M. Sheik-Bahae, Precision, all-optical measurement of external quantum efficiency in semiconductors, *J. Appl. Phys.* **109**, 093108 (2011).
- [9] A. Ziabari, M. Zebarjadi, D. Vashaee, and A. Shakouri, Nanoscale solid-state cooling: A review, *Rep. Prog. Phys.* **79**, 095901 (2016).
- [10] E. L. Murphy and R. H. Good, Thermionic emission, field emission, and the transition region, *Phys. Rev.* **102**, 1464 (1956).
- [11] G. Hatsopoulos and E. Gyftopoulos, *Thermionic Energy Conversion. Volume II. Theory, Technology, and Application* (MIT Press, Cambridge, MA, 1979).
- [12] G. D. Mahan, Thermionic refrigeration, *J. Appl. Phys.* **76**, 4362 (1994).
- [13] A. Shakouri and J. E. Bowers, Heterostructure integrated thermionic coolers, *Appl. Phys. Lett.* **71**, 1234 (1997).
- [14] T. Zeng and G. Chen, Interplay between thermoelectric and thermionic effects in heterostructures, *Microscale Thermophys. Eng.* **4**, 39 (2000).
- [15] G. D. Mahan and L. M. Woods, Multilayer Thermionic Refrigeration, *Phys. Rev. Lett.* **80**, 4016 (1998).
- [16] J. Zhang, N. G. Anderson, and K. M. Lau, Al<sub>0.10</sub>/Ga<sub>0.90</sub>/As-GaAs microcoolers, *IEEE Electron. Device Lett.* **25**, 345 (2004).
- [17] D. Vashaee and A. Shakouri, Improved Thermoelectric Power Factor in Metal-Based Superlattices, *Phys. Rev. Lett.* **92**, 106103 (2004).
- [18] M. Bescond, D. Logoteta, F. Michelini, N. Cavassilas, T. Yan, A. Yangui, M. Lannoo, and K. Hirakawa, Thermionic cooling devices based on resonant-tunneling AlGaAs/GaAs heterostructure, *J. Phys.: Condens. Matter* **30**, 064005 (2018).
- [19] A. Yangui, M. Bescond, T. Yan, N. Nagai, and K. Hirakawa, Evaporative electron cooling in asymmetric double barrier semiconductor heterostructures, *Nat. Commun.* **10**, 1 (2019).
- [20] S. Datta, *Electronic Transport in Mesoscopic Systems* (Cambridge University Press, Cambridge, U.K., 1995).
- [21] H. Haug and A.-P. Jauho, *Quantum Kinetics in Transport and Optics of Semiconductors*, of Springer Series in Solid-State Sciences Vol. 123 (Springer, Berlin, New York, 1996).
- [22] N. Cavassilas, F. Michelini, and M. Bescond, Modeling of nanoscale solar cells: The green's function formalism, *J. Renew. Sustain. Energy* **6**, 011203 (2014).
- [23] D. K. Ferry and S. M. Goodnick, *Transport in Nanostructures* (Cambridge University Press, Cambridge, U.K., 1997).
- [24] A. Price and A. Martinez, Electrothermal simulations of Si and III-V nanowire field effect transistors: A



- non-equilibrium green's function study, *J. Appl. Phys.* **12**, 6670 (2015).
- [25] R. Lake, G. Klimeck, R. C. Bowen, C. Fernando, T. Moise, Y. C. Kao, and M. Leng, Interface roughness, polar optical phonons, and the valley current of a resonant tunneling diode, *Superlattices Microstruct.* **20**, 279 (1996).
- [26] S. Jin, Y. J. Park, and H. S. Min, A three-dimensional simulation of quantum transport in silicon nanowire transistor in the presence of electron-phonon interactions, *J. Appl. Phys.* **99**, 123719 (2006).
- [27] Y. Lee, M. Lannoo, N. Cavassilas, M. Luisier, and M. Bescond, Efficient quantum modeling of inelastic interactions in nanodevices, *Phys. Rev. B* **93**, 205411 (2016).
- [28] A. Svizhenko and M. P. Anantram, Role of scattering in nanotransistors, *IEEE-Trans. Electron. Dev.* **50**, 1459 (2003).
- [29] Jie Lai and Arun Majumdar, Concurrent thermal and electrical modeling of sub-micrometer silicon devices, *J. Appl. Phys.* **79**, 7353 (1996).
- [30] M. Bescond, H. Carrillo-Nunez, S. Berrada, N. Cavassilas, and M. Lannoo, Size and temperature dependence of the electron-phonon scattering by donors in nanowire transistors, *Solid State Electron.* **122**, 1 (2016).
- [31] M. Moussavou, M. Lannoo, N. Cavassilas, D. Logoteta, and M. Bescond, Physically Based Diagonal Treatment of Polar Optical Phonon Self-Energy: Performance Assessment of III-V Double-Gate Transistors, *Phys. Rev. Appl.* **10**, 064023 (2018).
- [32] I. Vurgaftman, J. R. Meyer, and L. R. Ram-Mohan, Band parameters for III-V compound semiconductors and their alloys, *J. Appl. Phys.* **89**, 5815 (2001).
- [33] M. S. Lundstrom, *Fundamentals of Carrier Transport* (Cambridge University Press, Cambridge, U.K., 2009).
- [34] R. Lake and S. Datta, Energy balance and heat exchange in mesoscopic systems, *Phys. Rev. B* **117**, 164501 (1992).
- [35] M. Lopez-Sancho, J. Lopez-Sancho, and J. Rubio, Quick iterative scheme for the calculation of transfer matrices: Application to Mo (100), *J. Phys. F: Met.* **14**, 1205 (1984).
- [36] A. Sood, J. A. Rowlette, C. G. Caneau, E. Bozorg-Grayeli, M. Asheghi, and K. E. Goodson, Thermal conduction in lattice-matched superlattices of InGaAs/InAlAs, *Appl. Phys. Lett.* **105**, 051909 (2014).
- [37] M. N. Luckyanova, J. A. Johnson, A. A. Maznev, J. Garg, A. Jandl, M. T. Bulsara, E. A. Fitzgerald, K. A. Nelson, and G. Chen, Anisotropy of the thermal conductivity in GaAs/AlAs superlattices, *Nano Lett.* **13**, 3973 (2013).
- [38] E. Pop, S. Sinha, and K. E. Goodson, in *SISPAD Tech. Dig.* (IEEE, Boston, Massachusetts, USA, 2003) p. 121.
- [39] Marco Pala and Alessandro Cresti, Increase of self-heating effects in nanodevices induced by surface roughness: A full-quantum study, *J. Appl. Phys.* **117**, 084313 (2015).
- [40] T. Luo, J. Garg, J. Shiomi, K. Esfarjani, and G. Chen, Gallium arsenide thermal conductivity and optical phonon relaxation times from first-principles calculations, *EPL* **101**, 16001 (2013).
- [41] W. S. Capinski, H. J. Maris, T. Ruf, M. Cardona, K. Ploog, and D. S. Katzer, Thermal-conductivity measurements of GaAs/AlAs superlattices using a picosecond optical pump-and-probe technique, *Phys. Rev. B* **59**, 8105 (1999).